Optimization of circular photonic crystal cavities – beyond coupled mode theory

Derek Chang, Jacob Scheuer and Amnon Yariv

Departments of Electrical Engineering and Applied Physics M/C 128-95,California Inst. of Technology, 1200 E. California Blvd. Pasadena, CA, 91125
koby@caltech.edu

Abstract: We study comprehensively using numerical simulations a new class of resonators, based on a circular photonic crystal reflector. The dependence of the resonator characteristics on the reflector design and parameters is studied in detail. The numerical results are compared to analytic results based on coupled mode theory. High quality factors and small modal volumes are found for a wide variety of design parameters.

OCIS codes: (230.5750) Resonators; (130.2790) Guided waves.

References and links

1. C. K. Madsen and J. H. Zhao, *Optical Filter Design and Analysis: A Signal Processing Approach*, (Wiley-Interscience, New York, 1999).
2. B. E. Little, "Second-order filtering and sensing with partially coupled traveling waves in a single resonator," Opt. Lett. **23,** 1570-1572 (1998).
3. A. Melloni, R. Costa, P. Monguzzi, and M. Martinelli, "Ring-resonator filters in silicon oxynitride technology for dense wavelength-division multiplexing systems," Opt. Lett. **28,** 1567-1569 (2003).
4. J. E. Heebner and R. W. Boyd, "'Slow' and 'fast' light in resonator-coupled waveguides," J. Mod. Opt **49,** 2629-2636 (2002).
5. A. Melloni, F. Morichetti, and M. Mertinelli, "Linear and nonlinear pulse propagation in coupled resonator slow-wave optical structures," Opt. Quantum Electron. **35,** 365 (2003).
6. J. Scheuer, G. T. Paloczi, J. K. S. Poon and A. Yariv, "Coupled Resonator Optical Waveguides: Towards Slowing and Storing of Light," Opt. Photon. News **16**, 36-40 (2005).
7. A. Yariv, "Critical coupling and its control in optical waveguide-ring resonator systems," IEEE Photonics Technol. Lett. **14,** 483-485 (2002).
8. C. Y. Chao and L. J. Guo, "Biochemical sensors based on polymer microrings with sharp asymmetrical resonance," Appl. Phys. Lett. **83,** 1527-1529 (2003).
9. See, for example, K. J. Vahala, "Optical microcavities," Nature (London) 424, 839-846 (2003), and references therein.
10. J. Vuckovic, M. Loncar, H. Mabuchi, and A. Scherer, "Design of photonic crystal microcavities for cavity QED," Phys. Rev. E **65**, 016608 (2001).
11. O. Painter, R. K. Lee, A. Scherer, A. Yariv, J. D. O'Brien, P. D. Dapkus and I. Kim, "Two-dimensional photonic band-gap defect mode laser," Science **284,** 1819-1821 (1999).
12. H. Y. Ryu , M. Notomi and Y. H. Lee, "High-quality-factor and small-mode-volume hexapole modes in photonic-crystal-slab nanocavities," Appl. Phys. Lett. **21,** 4294-4296 (2003).
13. H. Y. Ryu , M. Notomi, G. H. Kim and Y. H. Lee, "High quality-factor whispering-gallery mode in the photonic crystal hexagonal disk cavity," Opt. Express **12,** 1708-1719 (2004), http://www.opticsexpress.org/abstract.cfm?URI=OPEX-12-8-1708.
14. Y. Akahane, T. Asano, B. S. Song and S. Noda, "High-Q photonic nanocavity in a two-dimensional photonic crystal," Nature **425,** 944-947 (2003).
15. B. S. Song, S. Noda, T. Asano and Y. Akahane, "Ultra-high-Q photonic double-heterostructure nanocavity," Nature Materials **4,** 207-210 (2005).
16. M. Lončar et al. "High quality factors and room-temperature lasing in a modified single-defect photonic crystal cavity," Opt. Lett. **29**, 721-723 (2004).
17. J. Scheuer and A. Yariv, "Annular Bragg Defect mode Resonators," J. Opt. Soc. Am. B. **20,** 2285-2291 (2003).

#8911 - $15.00 USD Received 27 September 2005; revised 31 October 2005; accepted 31 October 2005

18. J. Scheuer and A. Yariv, "Coupled-Waves Approach to the Design and Analysis of Bragg and Photonic Crystal Annular Resonators," IEEE J. Quantum Electron. **39,** 1555-1562 (2003).
19. J. Scheuer and A. Yariv, "Circular photonic crystal resonators," Physical Review E **70,** 036603 (2004).
20. J. Scheuer, W. M. J. Green, G. DeRose and A. Yariv, "Low Threshold Two-Dimensional Annular Bragg Lasers," Opt. Lett. **29,** 2641-2643 (2004).
21. J. Scheuer, W. M. J. Green, G. DeRose and A. Yariv, "InGaAsP annular Bragg lasers: Theory, applications and modal properties," IEEE J. Sel. Top. Quantum Electron. **11,** 476-484 (2005).
22. K. Srinivasan and O. Painter, "Momentum space design of high-Q photonic crystal optical cavities," Opt. Express **10,** 670-684 (2002), http://www.opticsexpress.org/abstract.cfm?URI=OPEX-10-15-670.
23. J. Vučkovič et al., "Optimization of the Q factor in photonic crystal microcavities," IEEE J. Quantum Electron. **38,** 850-856 (2002).
24. J. Scheuer, W. M. J. Green, G. DeRose and A. Yariv, "Lasing from a circular Bragg nanocavity with and ultrasmall modal volume," Appl. Phys. Lett. **86,** 251101 (2005).
25. G. N. Watson, *Theory of Bessel Functions*, 2nd ed. (London, U.K. Cambridge Univ. Press, 1952).
26. G. Mur, "Absorbing boundary conditions for the finite-difference approximation of the time-domain electromagnetic-field equations," IEEE Tansactions on Electromagnetic Compatibility **EMC-23**, 377-382 (1981).

1. Introduction

Circular optical resonators are becoming key components in modern optical communication systems and devices. Numerous applications for optical communications have been demonstrated such as filters [1], add/drop multiplexers [2, 3], delay lines [4-6] and modulators [7] as well as for sensing [8], spectroscopy and basic research in quantum electrodynamics (QED), nonlinear optics and similar fields [9, 10].

For many of these applications, it is desirable for the resonators to exhibit both compact dimensions and high quality factor (Q), which is a measure of the power dissipation rate from the cavity. These requirements are mutually contradictory for conventional resonators utilizing the total internal reflection (TIR) mechanism to confine the light. While for cavity radii much larger than the wavelength, high Q can be achieved, as the radius is reduced, the effectiveness of the TIR mechanism decreases, introducing loss which consequently reduces the Q of the cavity. This loss mechanism is often addressed as "bending losses".

This link between the bending losses and the cavity dimensions can be broken in resonators employing distributed Bragg reflection instead of TIR. Such resonators, e.g., Photonic Crystal (PC) defect cavities [11-16] and Circular Bragg resonators [17-21] have been suggested and studied before, demonstrating ultra-small modal volume and high Q although not as high as demonstrated in other types of cavities. Consequently, significant efforts were devoted to improving the Q of PC cavities. Generally speaking, the cavity Q can be separated into two contributions – the in-plane or horizontal Q ($Q_{||}$) and the out-of-plane or vertical Q ($Q_{\perp}$) associated with the power radiating from resonator in the slab plane and perpendicular to the slab plane respectively. While the in-plane losses (determining $Q_{||}$) can be, in principle, arbitrarily reduced by increasing the length of the reflector (the number of Bragg layers), the out-of-plane losses are more complicated to minimize. It has been shown, that the out-of-plane Q can be improved by rearranging the positions and dimensions of the holes of the PC reflector to reduce the intensity of the field components lying within the light cone [22, 23]. The idea underlying the optimization process is to "soften" the edge of the cavity in order to construct a more "smooth" field profile [15]. Nevertheless, such optimization requires a tedious procedure of tailoring the position and size of each hole in the PC reflector.

Recently, it was suggested to employ radial Bragg layers instead of PC to confine light in small cavities [24]. The radial structure offers significant advantages for optimal cavity design, primarily because it enables analytic design of the layer structure and optimal tailoring of the cavity size and the reflector periodicity. Unfortunately, the radial Bragg structure is

#8911 - $15.00 USD Received 27 September 2005; revised 31 October 2005; accepted 31 October 2005

difficult to realize using the suspended membrane concept which was successfully used for PC cavities. In addition, the upper surface of such structure is not continuous which makes it less suitable for electrical pumping and for realizing electrically pumped micro-lasers. To facilitate that, a new type of circular resonator based on PC reflectors was proposed [17, 18] (see Fig. 1). The generic structure consists of a solid disk surrounded by a perforated area of holes which serves as a distributed feedback reflector (DBR). Such structure can be realized using the suspended membrane concept and to be electrically pumped while retaining the advantages of the circular geometry.

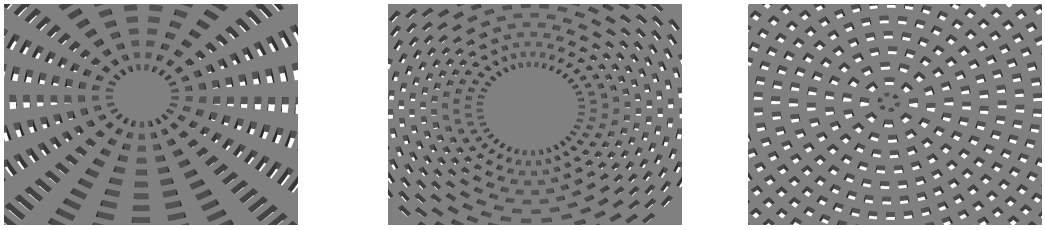

(1a) (1b) (1c)

Fig. 1. Circular PC reflector structure. (a) rectangular lattice (b) triangular lattice (c) sunflower lattice

In this paper, we use three-dimensional Finite Difference Time Domain (FDTD) simulations to comprehensively study circular PC resonator structures. The generic structure is shown in Fig. 1. The arrangement of the holes defines the type of the reflector. Specifically, we focus on three different types of structures: the rectangular lattice (Fig. 1a), the triangular lattice (1b) and the "sunflower" lattice (1c). The rectangular lattice structure is a cylindrical counterpart of the rectangular PC in Cartesian coordinates. Each "necklace" consists of identical number of holes and the angular length of the holes increases for larger radii. The holes in the triangular lattice structure are arranged in a similar way but with a half period shift in the azimuthal direction. The sunflower lattice structure comprises holes of the same angular size where the number of holes in each concentric ring is proportional to the circumference of the ring.

In section 2, we briefly discuss the design of our structures, in section 3 we present the studied structure and the results obtained from the FDTD simulations, and in section 4 we discuss the results and summarize.

2. Structural design

We consider a resonator structure of the type shown in Fig. 1. These structures consist of two regions: 1) A solid dielectric disk and 2) A perforated area which serves as a distributed feedback reflector. Because of the cylindrical geometry, the TM modal field solution in the central disk is a superposition of the Hankel functions of the first and second kind [25]:

$$H_z(x) = A \cdot H_m^{(1)}(x) + B \cdot H_m^{(2)}(x) \tag{1}$$

where H_z is the z component of the magnetic field, $H_m^{(1,2)}$ are respectively the m^{th} order Hankel functions of the first and second kind, $x = k_0 n_{eff} \rho$ is the normalized radius, k_0 is the wavenumber in vacuum, ρ is the radial coordinate, and n_{eff} is the effective index of the slab in the vertical dimension (this parameter is used in order to reduce the 3D problem to an effective 2D one). In the spirit of coupled mode theory (CMT), the field profile in the perturbed region can be represented in a similar fashion where the amplitudes A and B vary slowly in x:

$$H_z(x) = A(x) \cdot H_m^{(1)}(x) + B(x) \cdot H_m^{(2)}(x) \tag{2}$$

#8911 - $15.00 USD Received 27 September 2005; revised 31 October 2005; accepted 31 October 2005

Following conventional derivation of CMT, it can be shown that the required dielectric profile for efficiently coupling between the outgoing ($H^{(1)}$) and incoming ($H^{(2)}$) waves is given by [19]:

$$\varepsilon(x,\theta)=\begin{cases} n_0^2-(n_0^2-n_p^2)\Im[2\varphi(H_m^{(1)}(x)),\alpha_r]\Im[l\theta,\alpha_\theta], & x>x_0 \\ n_0^2, & x\le x_0 \end{cases} \tag{3a}$$

$$\Im(y,\alpha)=\begin{cases} 0, & \sin(y)<\alpha \\ 1, & \sin(y)\ge\alpha \end{cases} \tag{3b}$$

where x_0 indicates the (normalized) radius of the inner disk, $-1<\alpha_r<1$, $-1<\alpha_\theta<1$, l is the angular (spatial) frequency of the perturbation, φ indicates the phase function and n_0 and n_p are respectively the material and "holes" indices of refraction. The parameters α_r and α_θ represent threshold levels that determine the angular and radial size of the holes in the reflector region where larger α's indicate smaller holes and, correspondingly, weaker perturbation.

The index structure (3) generates a circular cavity with a rectangular photonic crystal reflector (Fig. 1(a)). The triangular and sunflower reflectors shown, respectively, in Figs. 1(b) and 1(c) can be constructed in a similar way by slightly modifying (3). In the triangular lattice, every second "necklace" of holes is rotated by a half of a cycle compared to the rectangular lattice and in the sunflower lattice, the number of holes in each "necklace" is increased linearly with the radius in order to retain the angular size of the holes. Other lattice configurations can be envisioned as well, e.g. lattices with random rotation of each "necklace" of holes, lattices with circular holes, etc. but the study of such configurations is beyond the scope of this paper. Nonetheless, it is important to note that from the CMT point of view, the angular dependence of the perturbation is of less significance and that it is the radial part of the perturbation which determines the modal field profile [18].

For the index profile (3), the radial mode profile consists of a Bessel function in the central disk and an exponentially decaying Bessel function in the reflector region [18]. The decay constant depends on the strength of the perturbation which is affected by the threshold levels α_r and α_θ:

$$H_z(x)=\begin{cases} J_m(x) & x<x_0 \\ J_m(x)\exp\left[-|k|(x-x_0)\right] & x\ge x_0 \end{cases} \tag{4}$$

where k is the coupling coefficient between the radially incoming and outgoing waves, given by $k=\Delta\varepsilon_0/\pi n_0^2$ and $\Delta\varepsilon_0$ is the DC component of the Fourier expansion of the reflector index profile. For the "rectangular" lattice (3), this component is given by:

$$\Delta\varepsilon_0=-2\cdot\left(n_0^2-n_p^2\right)\cos[\sin^{-1}(\alpha_r)]\cdot\cos^{-1}(\alpha_\theta)/\pi^2 \tag{5}$$

Equation (5) illustrates the impact of the various parameters on the coupling coefficient and, correspondingly, on the radial mode profile (4). As can be expected, decreasing α_r and α_θ results in a stronger coupling coefficient and a more confined mode profile. Although (3a) represents the index profile of the "rectangular" reflector, it can be straightforwardly shown that the coupling coefficients of the "triangular" and "sunflower" reflectors are identical (for the same values of α_r and α_θ – see [19] for more details).

3. Simulation results

In our simulations, we consider a 0.3 μm thick dielectric slab with refractive index of 3.4 suspended in air. For the TM (H_z) polarization, this configuration yields a vertical effective index of 2.86 at the design wavelength of 1.55μm. The radius of the inner disk is 1 μm and the reflector covers the rest of the horizontal computation area. We designed the dimensions

#8911 - $15.00 USD Received 27 September 2005; revised 31 October 2005; accepted 31 October 2005

of our structure for the 8th angular mode (m=8). The computation volume is 10.6 μm x 10.6 μm x 2.1 μm. The spatial and temporal resolutions of our simulations are respectively 26.5 nm and 0.08 fs. The simulation time interval is approximately 60 ps. The structure is excited with a short, broad-band, pulse (~2ps), and second order Mur absorbing boundary conditions [26] are employed to reduce the influence of reflections from the computation boundaries

We are primarily interested in four different aspects of the resonator structure and how they affect the Q, the resonance wavelength and the modal volume. The quality factor is evaluated according to $Q = \omega_0\tau_0$ where ω_0 is the resonant frequency and τ_0 is the cavity ring-down time constant. Both quantities (ω_0 and τ_0) are directly extracted from the FDTD simulation. Among the three lattice types presented above, we focus on the sunflower reflector because both 2D and 3D simulations predict superior Q for this type of lattice [19].

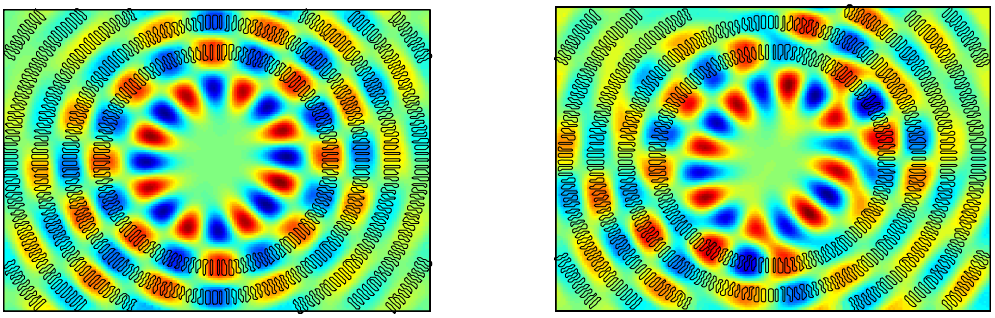

(a) (b)

Fig. 2. Field Profile of (a) high Q and (b) low Q for a "sunflower" resonator with l=70, α_r=0 and α_θ=0.1

Figure 2 depicts a cross-section of the z component of the magnetic field (H_z) at the center of the slab at t = 60ps. It illustrates the difference between a field profile with high Q and one with low Q for a "sunflower" structure with l=70, α_r=0 and α_θ=0.1. In Fig. 2a, the high Q field is symmetric and well confined to the center of the disk. The low Q field shown in Fig. 2b exhibits distortion due to beating between two close resonance frequencies, but more importantly, the field is not well confined and therefore exhibits more loss.

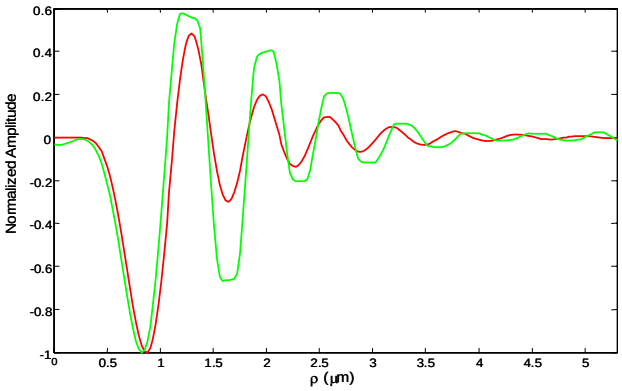

Fig. 3. Comparison between theoretical (red) and numerical (green) radial field profile

In Fig. 3, we compare the numerically calculated radial mode profile (green) with the analytical solution (red). The analytical solution is given by (4). While the analytic oscillation (quasi) periodicity seems to agree reasonably well with the calculated one, the decay rates differ significantly. We attribute this difference to the fact that the profile (4) is

#8911 - $15.00 USD Received 27 September 2005; revised 31 October 2005; accepted 31 October 2005

accurate only for small perturbations [19] while the index perturbations of the simulated structure are rather strong.

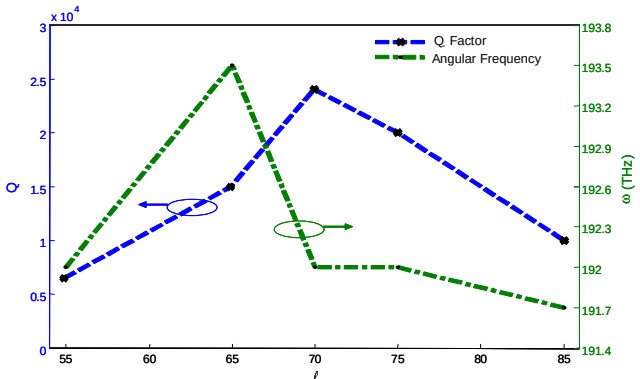

Fig. 4. Quality factor and resonance (angular) frequency vs. Angular Perturbation

Figure 4 depicts the dependence of the resonance frequency (green) and the Q (blue) on the angular perturbation frequency. α_θ and α_r are maintained fixed at 0 and 0 respectively. The x-axis indicates the number of holes in the first "necklace" (fig. 1c). While the resonance frequency is relatively insensitive to the angular perturbation frequency, the Q of the resonator varies significantly when this frequency is changed. The Q reaches a peak value of about Q = 25,000 around l = 70 and decreases significantly for both smaller and larger l. Two-dimensional simulations [19] showed that the Q is expected to increase with l. We attribute this trend to the fact that smaller holes generate a more homogeneous angular perturbation which is closer to the ideal case of concentric rings. Therefore, we believe that the decrease in the Q observed for l > 70, is a numerical artifact stemming from the limited resolution of the numerical scheme. The modal volumes of the structures with l = 65, 70 and 75 are respectively 3.8, 4.6 and 3.8 cubic wavelengths. It can therefore be seen that while the Q is significantly affected by l, its impact on the modal volume is rather small.

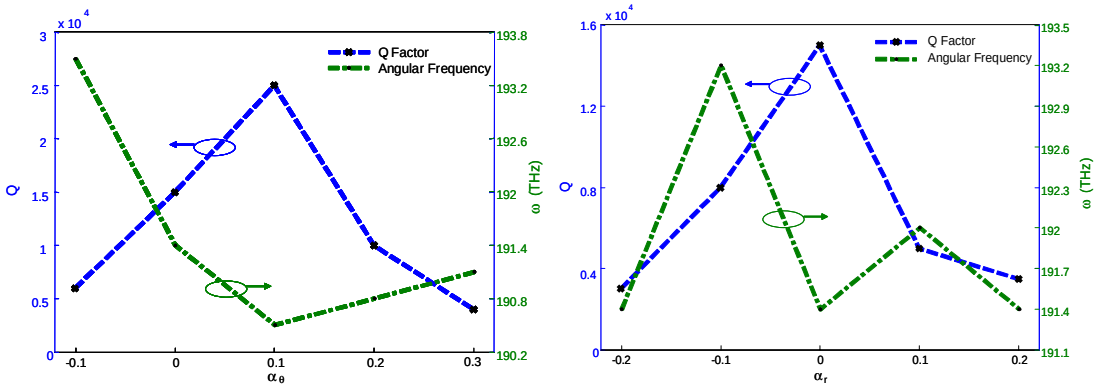

(a) (b)

Fig. 5. Dependence of the Q and resonant frequency on (a) α_θ and (b) on α_r

As discussed in section II, the perturbation profile is determined by two parameters: α_θ, which determines the duty-cycle of the angular dependence of the perturbation and α_r, which, roughly speaking, determines the duty cycle of the radial dependence of the perturbation. In particular, α_θ and α_r represent generalized threshold levels that determine the transition from high-index to low-index. The values of α_r and α_θ determine the size of the holes where the

#8911 - $15.00 USD Received 27 September 2005; revised 31 October 2005; accepted 31 October 2005

larger α_θ and α_r, the smaller the holes. α_θ and α_r affect the overall size of the holes which have opposite impact on the vertical and horizontal losses. Larger holes (smaller α_r and α_θ) reduce the in-plane radiation losses but also generate more Fourier components which are above the light-cone, and thus, increase the out-of-plane (vertical) scattering. Correspondingly, smaller holes (softer perturbation) reduce the vertical scattering but also the horizontal confinement resulting in larger in-plane losses for a fixed external radius of the reflector. Consequently, for a device with fixed external radius, there are optimal α_θ and α_r for which the total *Q* is maximal.

Figure 5(a) shows the dependence of the *Q* and the resonance frequency on α_θ while α_r is fixed at 0. A large *Q* is found for $\alpha_\theta = 0.1$. Figure 5(b) shows the dependence of the *Q* and resonance frequency on α_r while α_θ is fixed at 0. Unlike the angular perturbation, which is periodic in $2\pi/l$ (see Eq. (3)), the radial perturbation is not exactly periodic because it is determined by the oscillations of the appropriate Hankel function. Similar to α_θ, there is an optimal value for α_r, in this case α_r is around 0, which is determined by the tradeoff between the horizontal and the vertical *Q*s. It should be emphasized that the optimal values for α_θ and α_r stem from the fixed external radius of the Bragg reflector. Increasing the reflector radius would improve the horizontal *Q* and would allow for larger α_θ (softer perturbation).

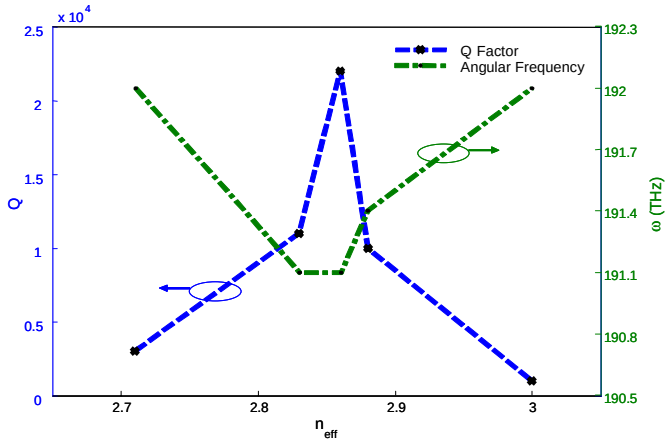

Fig. 6. Impact of n_{eff} on the *Q* and resonant frequency

Finally, we examine the impact of the effective index (n_{eff}) on the *Q* and resonance frequency while fixing l=65, α_r=0 and α_θ=0.1. n_{eff} is a design parameter which stems from the reduction of the 3D problem to an equivalent 2D problem. To determine the holes position, the slab configuration is replaced by an equivalent 2-D structure with an effective index, n_{eff}, determined by the vertically guided mode of the slab. It is, therefore, important to verify the validity of this approximation by varying the value of n_{eff} used in the design of the cavity. Figure 6 shows the impact of changing n_{eff} in (3) on the *Q* and resonance frequency. The maximal *Q* is found for $n_{eff} = 2.86$, which is the effective index of the guided mode in the slab, thus indicating that the effective index approximation is valid and can be used for the design of such cavities.

4. Conclusion

We studied the impact of the various design parameters of circular PC cavities on their *Q*, modal volume and resonance frequency using 3D FDTD simulations. For a fixed size resonator, there is a clear tradeoff between the vertical and horizontal *Q*s manifested in optimal α_r and α_θ. We also found that increasing the angular (spatial) frequency of the perturbation generally increases the *Q* up to a limit which, most probably, stems from

#8911 - $15.00 USD Received 27 September 2005; revised 31 October 2005; accepted 31 October 2005

numerical errors generated by the limited resolution of the calculation scheme. We attribute this trend to the fact that higher perturbation frequencies generate smaller holes which reduces the local perturbation and the scattering losses, without affecting the radial coupling coefficient which confines the light in the central cavity. We also studied the influence of the effective index approximation used for the design procedure and found that the best *Q* is attained when the actual slab effective is used for the design, thus validating the use of this approximation. Good agreement was found between the analytically and the numerically calculated radial field profile, even for relatively strong perturbation, indicating that the design and analysis method used here accurately describes the actual structure. The small number of design parameters and degrees of freedom (compared to PC defect cavities) allow for a thorough engineering of the cavity structure, yielding high *Q*s and small modal volumes.

Acknowledgments

The authors would like to acknowledge the support of the National Science Foundation and DARPA. D. Chang acknowledges the support of the SURF program. J. Scheuer acknowledges the support of the Information Science and Technology center at Caltech.

#8911 - $15.00 USD Received 27 September 2005; revised 31 October 2005; accepted 31 October 2005